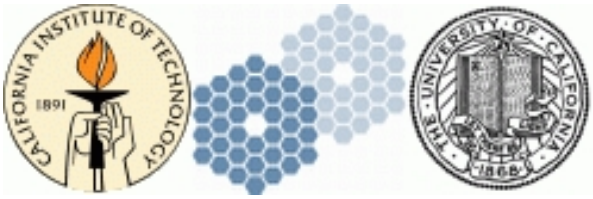

Astrometry for NGAO
Keck Adaptive Optics Note 480

Brian Cameron, COO
Matthew Britton, COO
Jessica Lu, UCLA
Andrea Ghez, UCLA
Richard Dekany, COO
Claire Max, UCSC
Chris Neyman, WMKO

May 3, 2007

1 Introduction

Adaptive optics (AO) are a powerful tool for performing narrow-field astrometry. AO increases the precision of positional measurements by shrinking the point-spread function (PSF) and boosting the signal-to noise ratio. These enhancements open up new phase space for astronomers. The possible astrometric experiments span a wide range of Galactic environments, from faint binary companions to crowded stellar fields in the inner Galaxy. In addition, AO increases the efficiency with which these projects can be carried out.

Unlike many other applications of AO, astrometrists are concerned with both the quality of the PSF delivered by the AO system and where that PSF falls. In principle, photon noise ($\lesssim 0.1\,\mathrm{mas}$), or in rare cases confusion, should be the limiting factor for positional measurements. However, the realization of these levels are difficult in practice.

The limits are set by a number systematic and random errors provided by the system optics and the atmosphere. Effects include geometric distortions, atmospheric refraction and tilt jitter. The relative importance of these effects vary depending on the observational setup, science target properties and project goals. Here we consider the major drivers of the astrometric performance budget and attempt (as best we can) to estimate their overall effect on astrometric accuracy.

Research into each of the systematic limitations above is ongoing, but we will summarize our current understanding of each in §2. In §3 we will discuss the astrometric performance currently achieved by two ongoing astrometry efforts with the current generation AO system at Keck followed by a summary in §4. Finally, we provide a list of recommendations for NGAO in §5.

2 Effects on Astrometry

In the case of a perfect detector and optical system without an atmosphere the astrometric accuracy and precision would be limited only by photon noise. For a mono-pupil telescope this is

$$\sigma_{\text{centroid}} = \frac{\lambda}{4\pi D}\frac{1}{SNR} = 350\,\mu\text{as}\left(\frac{\lambda}{2.1\mu\text{m}}\right)\left(\frac{10\,\text{m}}{D}\right)\left(\frac{10}{SNR}\right) \quad (1)$$

where λ is the monochromatic wavelength of the observations, D is the telescope diameter, and SNR is the achieved signal-to-noise ratio [1]. However, this adding physical detector causes uncertainty due to variability in the individual pixel response functions. The addition of a physical optics adds optical distortions. Finally, ground-based facilities must contend with the atmospheric effects of refraction and uncorrected atmospheric tilt. We discuss each of these effects in the following sections.

2.1 Differential Tilt Jitter

Wavefronts propagating through the atmosphere to arrive at a telescope acquire random phase fluctuations from atmospheric turbulence. These phase fluctuations evolve in time as wind carries atmospheric turbulence past the telescope aperture. The tilt component of this random phase gives rise to atmospheric tilt jitter. This effect is apparent as a random jitter in the centroid of an image formed by the telescope. For atmospheric turbulence obeying a Kolmogorov power law spectrum and for a circular aperture, the 2 axis tilt variance T_z is given by

$$T_z^2 = \frac{6.08\mu_0}{D^{1/3}} \quad (2)$$

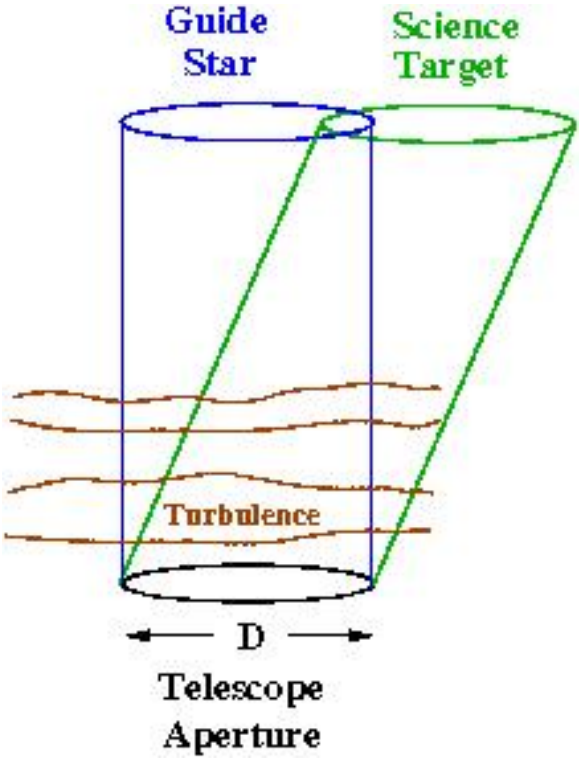

Figure 1: Anisoplanatism and differential tilt jitter. The effect of anisoplanatism arises from the fact that light from stars at finite angular separation traverse different columns of atmospheric turbulence. This results in differential tilt jitter among objects distributed over the field of view.

where D is the telescope aperture diameter and the turbulence moment μ_m is defined as

$$\mu_m = \int_0^\infty dz C_n^2(z) z^m \tag{3}$$

Thus, short exposure images of a star acquired under these turbulence conditions would display a random wander in the centroid position, which is described by a Gaussian distribution with a width of T_z. The typical timescale for temporal evolution of the wavefront tilt and centroid position is the wind crossing time, which is of order 1 sec. For the C_n^2 turbulence profile used in the NGAO system design, the atmospheric tilt jitter is 177 mas.

If the centroids of stars within a field of view are measured simultaneously, the measurements will display a degree of correlation that arises from the fact that wavefronts

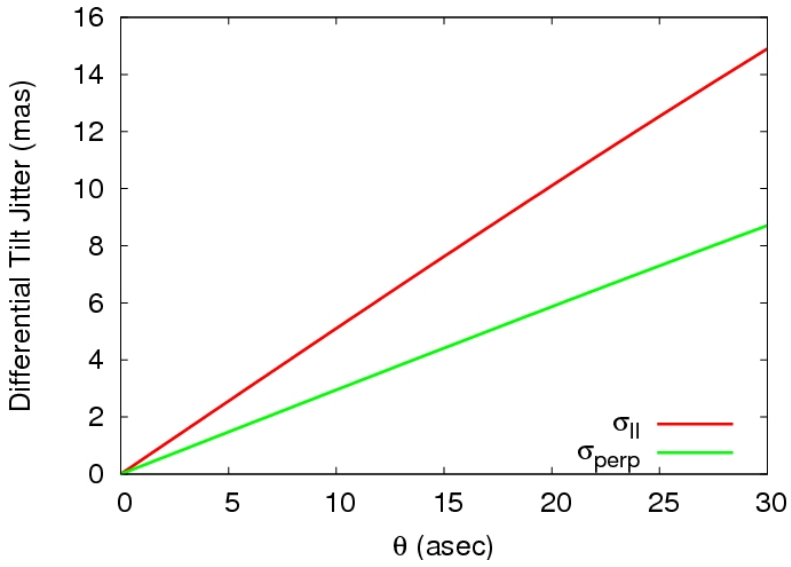

Figure 2: Plot of the parallel and perpendicular components of differential tilt jitter, $\sigma_{\parallel}$ and $\sigma_{\perp}$ as a function of angular offset θ between two stars. These results were computed using the C_n^2 profile adopted in the NGAO system design study. This movie shows the evolution of differential tilt jitter over a single night on Mauna Kea. The degree of differential tilt jitter evolves significantly in time due to temporal evolution of the C_n^2 profile. The C_n^2 profile measurements acquired by the TMT DIMM/MASS unit on Mauna Kea were used in generating this movie.

from these stars have propagated through the same realization of atmospheric turbulence. The geometry is shown in Figure 1, which displays the effect of shearing between the columns of atmospheric turbulence sampled by wavefronts from two stars at finite angular offset. The degree of correlation decreases with increasing angular offset. Often, astrometric applications require only the differential angular offsets among stars in the field. These differential measurements display scatter arising from differential tilt jitter, which arises from the shearing effect shown in Figure 1. This effect is anisotropic, in that the scatter along the direction defined by the separation axis is larger than that in the transverse direction. A three term approximation that describes the differential tilt variance arising from this effect is given by

$$\begin{bmatrix} \sigma_{\parallel}^2 \\ \sigma_{\perp}^2 \end{bmatrix} = 2.67 \frac{\mu_2}{D^{1/3}} \left(\frac{\theta}{D}\right)^2 \begin{bmatrix} 3 \\ 1 \end{bmatrix} - 3.68 \frac{\mu_4}{D^{1/3}} \left(\frac{\theta}{D}\right)^4 \begin{bmatrix} 5 \\ 1 \end{bmatrix} + 2.35 \frac{\mu_{14/3}}{D^{1/3}} \left(\frac{\theta}{D}\right)^{14/3} \begin{bmatrix} 17/3 \\ 1 \end{bmatrix} \quad (4)$$

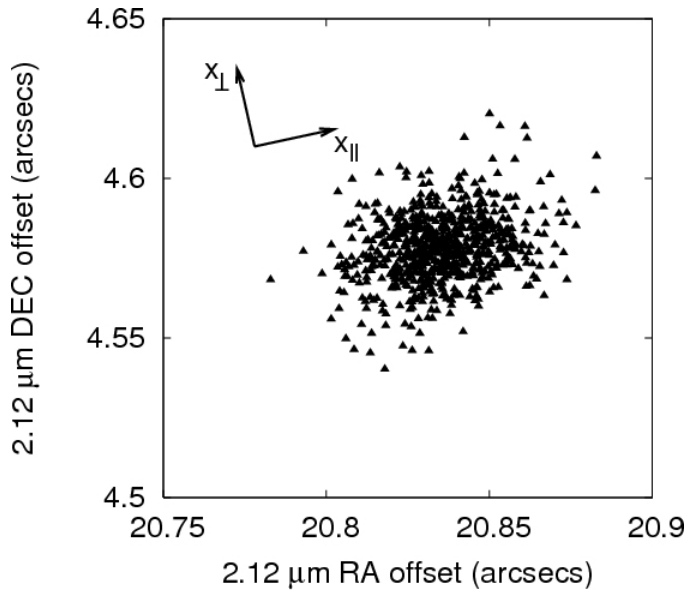

Figure 3: Effects of differential tilt jitter on measurements of the separation between two binary members. The plot displays measurements of the vector separation between members of a 21 asec binary in a sequence of about seven hundred 1.4 sec exposures taken with the PALAO system. The scatter arising from differential tilt jitter is predicted from theory to be larger along the binary axis, which is indicated in the plot by $x_{\parallel}$.

In this expression, the tilt variance parallel and perpendicular to the separation axis are denoted as $\sigma_{\parallel}$ and $\sigma_{\perp}$, while θ is the angular separation between the two stars. The turbulence moments μ_m are as defined in Equation 3. Figure 2 shows the differential tilt jitter vs. angular separation θ predicted for a 10 meter telescope observing through the C_n^2 profile adopted for the NGAO system design study.

The current generation of single conjugate adaptive optics systems used in astronomy correct for atmospheric tilt jitter by measuring the tilt of a natural guide star wavefront and applying this measurement to a tip tilt mirror. This technique is used for both natural and laser guide star AO systems. This type of tilt correction acts to stabilize the guide star, but measurements of the angular displacement between this star and other stars in the field will display scatter due to differential tilt jitter. These effects are clearly apparent in current datasets, and an example is shown in Figure 3. This effect will decrease with integration time as $\sqrt{t}$.

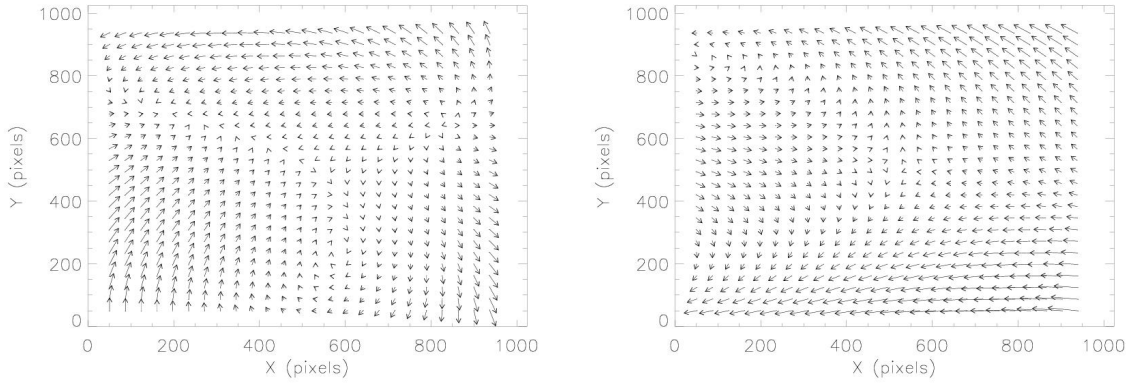

Figure 4: Measured optical distortion in the NIRC2 narrow camera (*Top*) and wide camera (*Bottom*) as a function of location on the chip. The largest errors near the chip edges indicate shifts of a few pixels.

2.2 Geometric Distortion

All optical systems suffer from image distortion. In the case of Keck, these distortions arise from the telescope, AO bench and the internal instrument optics. There are several strategies that can minimize the effects of these distortions. If they are static, the observations can be made in repeated fashion from epoch-to-epoch (e.g. repeated field is alignment relative to chip, dither patterns, etc.). These techniques have been used with great success for relative astrometry (see §3.1). However, such strategies will are not viable for heterogeneous data sets (e.g. combination with *Hubble* data or other instruments). In these cases, correction for geometric distortion is necessary to place the positional measurements in a global astrometric reference frame.

The geometric distortion in the NIRC2 wide (40 mas pixel^{-1}) and narrow (10 mas pixel^{-1}) has been characterized using a images of an illuminated grid of holes drilled in to a fused silica. The grid was machined to relatively high precision ($\approx 1\,\mu$m), and thus should be an excellent reference grid with which to measure distortion in the NIRC2 optics. The measured distortion in each camera can be seen in Figure 4. A polynomial is fit to this surface that can be applied to stellar positions to correct the geometric distortion. The residuals after the application of this solution are ≈ 0.09 pixels (≈ 3.6 mas) and ≈ 0.06 pixels (≈ 0.6 mas) in each axis of the wide and narrow cameras, respectively. The results of this work can be found on the NIRC2 news page.

Monitoring of these solutions from the beginning to the end of 2006B shows the solu-

Comparison of Separation and Color Effects

z_1 (deg)	ΔR K-band 2.0–2.4 μm (μas)	ΔR K'-band 2.0–2.33 μm (μas)	ΔR H-band 1.5–1.8 μm (μas)
$T_1 = T_2 = 5800\,\mathrm{K}$, $\Delta z_0 = 15$"			
0	3345.67	3345.78	3348.77
10	3449.29	3449.40	3452.49
20	3787.12	3787.24	3790.63
30	4455.77	4455.91	4459.90
40	5687.65	5687.82	5692.92
$T_1 = 5800\,\mathrm{K}$, $T_2 = 2800\,\mathrm{K}$, $\Delta z_0 = 15$"			
0	0.00	0.00	0.00
10	49.47	36.38	126.99
20	102.11	75.08	262.10
30	161.94	119.07	415.67
40	235.28	172.98	603.90

Table 1: For standard atmospheric parameters: $T = 278\,\mathrm{K}$, $P = 800\,\mathrm{mb}$ and $H = 10\%$.

tions are stable within the measurement errors Since these solutions are stable, at least for the NIRC2 optics, and show now positional dependence on the chip they can be averaged down as the square root of the number of dither positions.

The optics upstream of NIRC2 have not yet been characterized. The telescope provides the AO system with a curved focal plane, which is corrected before delivery to NIRC2 (KAON 309,314). The degree to which this correction is accurate will be the subject of upcoming off and on-sky testing in July, 2007.

2.3 Atmospheric Refraction

An important systematic effect to consider for precision astrometry is the apparent change in stellar positions that result from atmospheric refraction. The measured zenith angle of an incoming ray, z_0, is less than that which would have been measured in the absence of the atmosphere. The actual zenith angle is $z = z_0 + R$. It is this quantity, R, that we wish to evaluate for each star in the field to compute the differential refraction between stars, ΔR.

Differential refraction has proven to be the main limiting systematic for some seeing-

Summary of Measurements Required to Achieve 10 μas Accuracy

Quantity	Required Accuracy
z_1 (arcsec)	$\approx 36^a$
Δz_0 (mas)	30^a
T (%)	0.2 (0.6 K)^b
P (%)	0.2 (1.6 mb)^c
H (%)	10^d
T_1, T_2 (K)	100–1700^e

Table 2: $^aT_1 = 5800\,\mathrm{K}$, $T_2 = 2800\,K$, $z_1 = 30°$, $\Delta z_0 = 15$", $T = 278\,\mathrm{K}$, $P = 800\,\mathrm{mb}$, $H = 10\,\%$.
$^bT_1 = 5800\,\mathrm{K}$, $T_2 = 2800\,K$, $z_1 = 30°$, $\Delta z_0 = 15$", $P = 800\,\mathrm{mb}$, $H = 10\,\%$.
$^cT_1 = 5800\,\mathrm{K}$, $T_2 = 2800\,K$, $z_1 = 30°$, $\Delta z_0 = 15$", $T = 278\,\mathrm{K}$, $H = 10\,\%$.
$^dT_1 = 5800\,\mathrm{K}$, $T_2 = 2800\,K$, $z_1 = 30°$, $\Delta z_0 = 15$", $T = 278\,\mathrm{K}$, $P = 800\,\mathrm{mb}$.
$^e z_1 = 30°$, $\Delta z_0 = 15$", $T = 278\,\mathrm{K}$, $P = 800\,\mathrm{mb}$, $H = 10\,\%$; varies with colors of respective stars.

limited ground-based astrometric surveys performed in visible light (e.g. [2]). The magnitude of this effect for a sample case can be seen in Table 1 (adapted from [3]), but for reference two stars with an effective temperature of 5800 K separated by 15" at a zenith angle of 30° will have their observed separation altered by ~ 4.5 mas in the K' band.

The refraction can be separated into two components; achromatic and chromatic. The former depends on stellar separation along the zenith direction and the latter depends on their relative colors. There are seven quantities that must be known in order to correct the refraction: the zenith angle of one star (z_1), the observed separation along zenith to the second star (Δz_0), the ground-based temperature (T), pressure (P) and relative humidity (H) and the effective stellar surface temperatures (T_1, T_2). The accuracy to which these values must be known for 10 μas astrometry is summarized in Table 2 (from [3]). These meteorological parameters are already measured to the reported precision at Keck, and the stellar temperatures can be determined with proper observing program design. Thus, the major uncertainty is how well atmospheric models characterize the atmosphere along a given line-of-sight (particularly at high airmass). The accuracy of these models requires detailed comparison with data, which is on going.

It should also be noted that this problem will receive significant attention from planned large scale synoptic surveys (e.g. Pan-STARRS and LSST), since well calibrated astrometric catalogs are among their primary data products (cf. [4]).

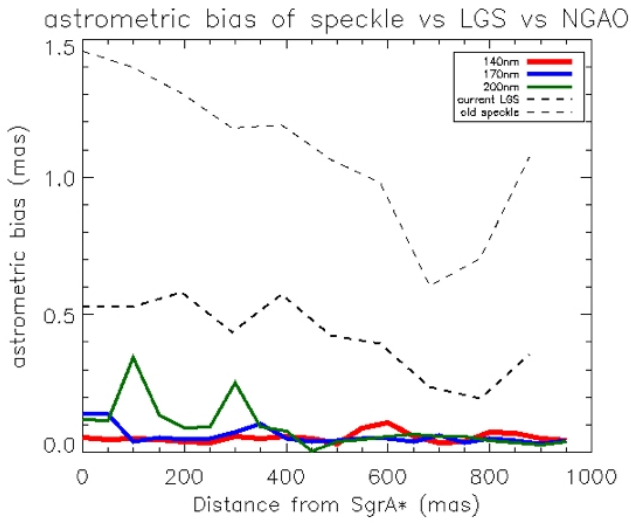

Figure 5: A comparison of the astrometric bias as a function of distance from the Galactic Center for a speckle data, current AO system and a number of WFE budgets. Note that the model PSFs for each WFE have been degraded to the relatively low elevation of the Galactic Center at Keck.

2.4 Confusion

In regions of very high stellar density (e.g. the inner 1" of the Galaxy) measurements of stellar positions are biased by the unresolved stellar background. This confusion can be increasingly mitigated with higher strehl ratios, namely lower wavefront error (WFE).

We have run preliminary simulations investigating the astrometric bias as a function of the WFE in the case of the Galactic Center. The results are shown in Figure 5. The astrometric goal for this science case is ≈ 0.1 mas, thus ≈ 140 nm of WFE is required to achieve this level of astrometric bias.

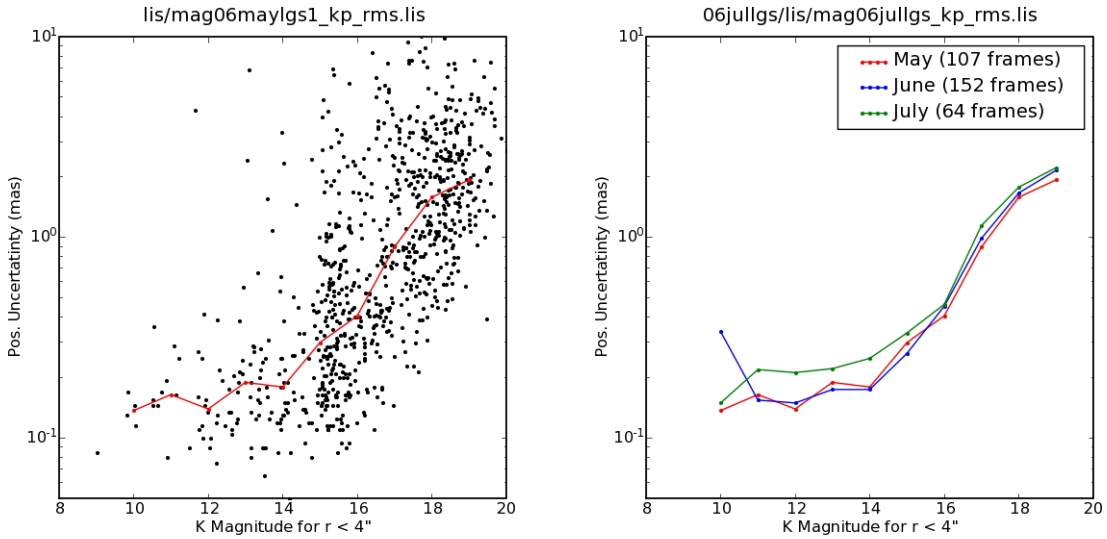

Figure 6: Position errors as a function of K-band magnitude in 2006 May (*Top*) and throughout 2006 (*Bottom*).

3 State of the Art: Science Applications and Performance

3.1 Case 1: The Galactic Center

Galactic center science requires good astrometric precision AND astrometric accuracy. The experiments that utilize astrometric measurements include determining the fundamental properties of the supermassive black hole (mass, position, distance), measuring the extended mass distribution, measuring general relativistic effects, determining the origin of young stars around the galactic center, and detecting hypervelocity stars being ejected from the galaxy. To perform these experiments requires measuring the positions of stars with high relative precision over several years in order to determine velocities, accelerations, and full orbits.

Current Galactic center observations at Keck II using the NIRC2 narrow camera achieve Strehl ratios of 0.3-0.4 and FWHM of 53-63 mas when the seeing conditions were characterized by $r_0 \approx 11$ cm and $\theta_0 \approx 1.3$" at an zenith angle of $\approx 60°$ (this corresponds to the zenith equivalent of $r_0 \approx 14$ cm and $\theta_0 \approx 2.7$"). Astrometric measurements are

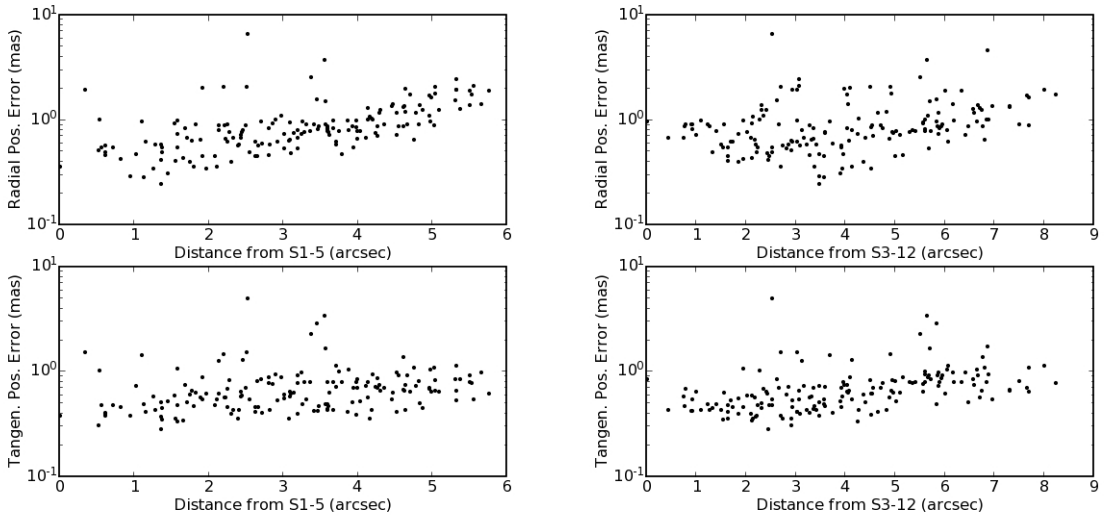

Figure 7: (*Top pair:* Positional uncertainty along radial and tangential directions with respect to a star at the center of the field of view. (*Bottom pair:*) Positional uncertainty along radial and tangential directions with respect to a star at near the edge of the field of view.

made by using *StarFinder* to determine the PSF empirically from stars in the field-of-view and then to extract source brightness and positions by fitting the PSF. Uncertainties are determined by dividing the data in a given night into 3 equal quality subsets, repeating the same analysis, and using the RMS of the positions in the subset images. Formally, the positional uncertainty includes both centroiding errors and image alignment errors since the subset images must be aligned; however, alignment error is small since it scales inversely with the number of stars used to align the images (≈700). The achieved astrometric precision as a function of K-band magnitude for ≈47 minutes of exposure time is shown in Figure 6. There appears to be an astrometric floor at which the positional uncertainties for the brightest stars are not set by the signal-to-noise of the measurement but rather by some as yet unidentified systematic effect. Positional uncertainties as low as 0.1 mas are measured for the brightest stars down to K∼15 mag. The fainter stars' positional uncertainties are limited by the signal-to-noise. Additionally, at a given magnitude, there is a substantial spread of positional uncertainties. This is most likely due to a number of factors including spatial variations in the PSF and confusion due to undetected sources. Figure 6 shows the average astrometric precision vs. magnitude for

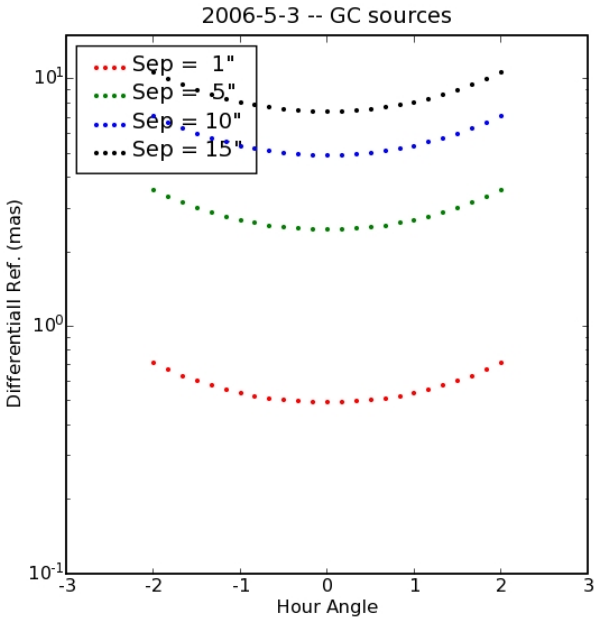

Figure 8: Achromatic portion of differential atmospheric refraction for the Galactic Center at a variety of separations.

several different nights.

The astrometric precision shows a strong dependence on field position. To fully characterize the field position dependence, a reference star was chosen near the center of the FOV (near where the laser is located) and the separation between the reference star and every other star in the field is computed. This is repeated for ≈180 individual exposures taken throughout the night and the RMS of the separation across all exposures is used as a measure of a stars positional uncertainty. Figure 7 shows this positional uncertainty as a function of radial distance from the reference source. The RMS of the separation can be decomposed into radial (along the axis of separation) and tangential (perpendicular to the axis of separation) components in order to look for isoplanatic effects which would be primarily along the radial direction. Positional uncertainty increases as a function of separation more along the radial direction but it also increases along the tangential direction as well. Plate scale changes could produce such a signature since a change in plate scale would uniformly stretch the image in all directions. Thus, if a different reference source was chosen, far from the center of the FOV, then the positional error vs.

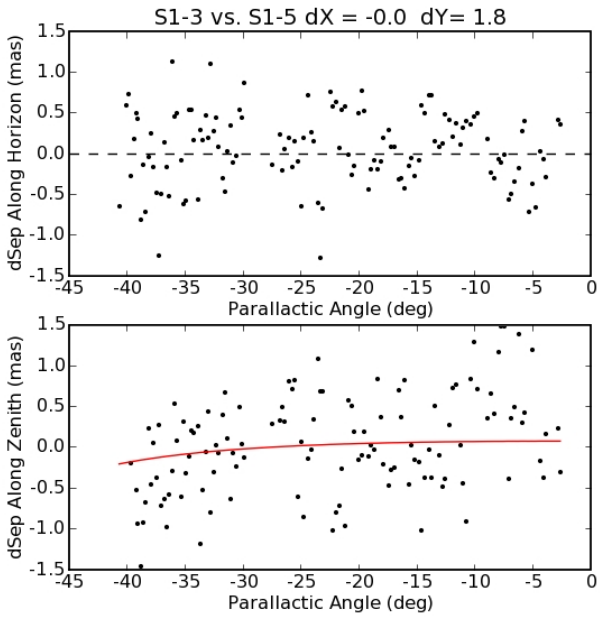

Figure 9: Separation between two nearby ($\lesssim$ 1") stars parallel to the horizon (*Top* and along the zenith direction (*Bottom*) as a function of parallactic angle.

separation should look the same. Figure 7 shows that this is not the case and that the lowest positional uncertainties always occur at the center of the FOV. Thus plate scale changes are not yet the dominant source of positional uncertainty.

Although our analysis is not yet complete, we suspect that the radially dependent positional uncertainty may be due to spatial variations in the PSF. This hypothesis is currently being explored, but visual inspection of the images shows that the PSF near the field edges is often elongated along the radial direction.

To test the new NIRC2 distortion solution as computed by the 2006 pinhole experiment (see §2.2), Galactic center data was analyzed with both the pre-ship review distortion solution and the new distortion solution for comparison. A data set with a large dither (6" $\times$ 6") was chosen to maximally sample the geometric distortion. Using the same pairwise analysis described above, the RMS of a star's separation was compared between the two different distortion solutions. Figure 11 shows the comparison along the detectors X and Y axes. A substantial improvement of nearly a factor of 2 is visible in the X axis using the new distortion solution. The Y axis appears to be unaffected.

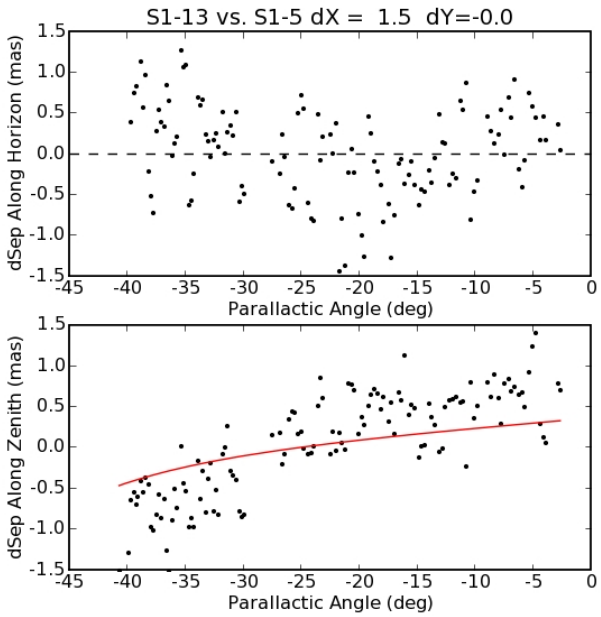

Figure 10: Separation between two stars (separation of a few arcseconds) stars parallel to the horizon (*Top* and along the zenith direction (*Bottom*) as a function of parallactic angle.

Differential atmospheric refraction (DAR) effects both the astrometric absolute accuracy and precision. Figure 8 shows the theoretical estimates for DAR during the Galactic center observations for stars at various separations. For two stars separated by 10", at transit, DAR changes the measured separation by 5 mas which should be accounted for when converting to an absolute astrometric reference frame. Additionally, DAR changes over the course of GC observations as the target changes airmass. For two stars separated by 10", there separations will change ≈1 mas over the course of a typical 3 hour observing window centered at transit. Currently, we do not correct for this effect (since it requires knowledge of atmospheric weather conditions) and thus this is a source of additional astrometric uncertainty. DAR effects only the separations along the zenith axis, so in order to investigate whether we can observe these effects in our astrometry, we performed a pairwise astrometry analysis decomposed along the zenith and horizon directions for each exposure. In each exposure, the stars' separation from the reference source, S1-5, was calculated and the difference between that separation and the average separation for that

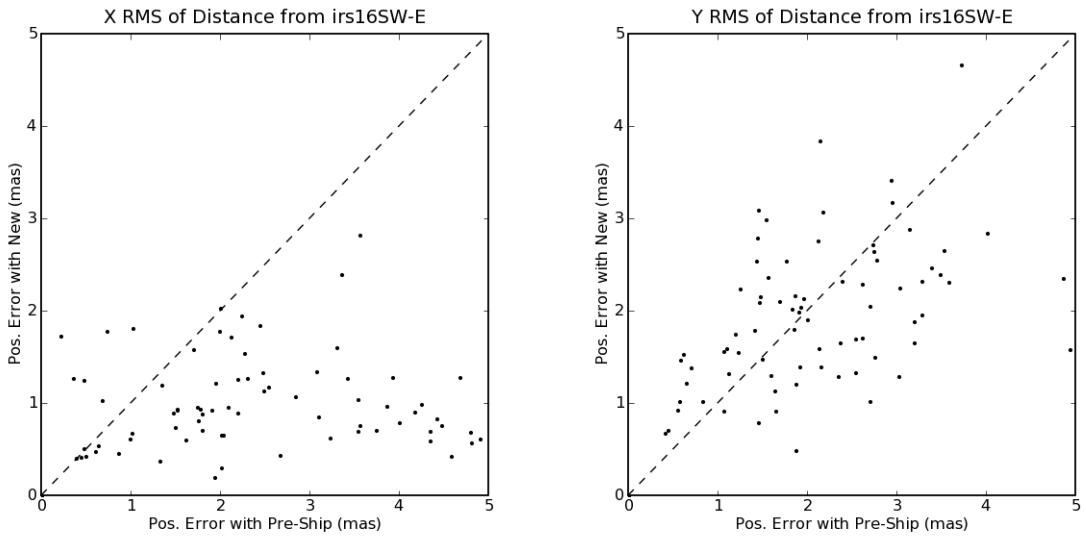

Figure 11: Comparison of the positional error of stars with preship and new distortion solutions along the x (*Top*) and y (*Bottom*) axes.

star for the entire night is plotted vs. parallactic angle in Figures 9-10. Figure 9 shows two stars with small separations. Figure 10 shows a star with a large horizon separation and a star with a large zenith separation. The red curves show the theoretical DAR effect for each star. The conclusion from this very preliminary analysis is that the stellar separations show systematic trends that are not consistent with DAR alone.

3.2 Case 2: Astrometry of Faint Isolated Targets

Modern near-infrared detectors and adaptive optics make it possible and highly attractive to undertake astrometry of objects in the Galactic plane. The location ensures an abundance of reference targets, which are critical for astrometry. Adaptive optics shrink the PSF, thereby improving precision and increasing signal-to-noise resulting in improved accuracy. Future astrometric missions like SIM and GAIA use optical detectors, and thus are not well suited for observing distant Galactic objects due to the high values of extinction. As such, these programs will remain unique.

One such project underway using Keck LGA-AO proposes to measure proper motions of various classes of compact objects (magnetars, nearby accreting black hole and neutron star systems). This experiment will address the formation, evolution and environments

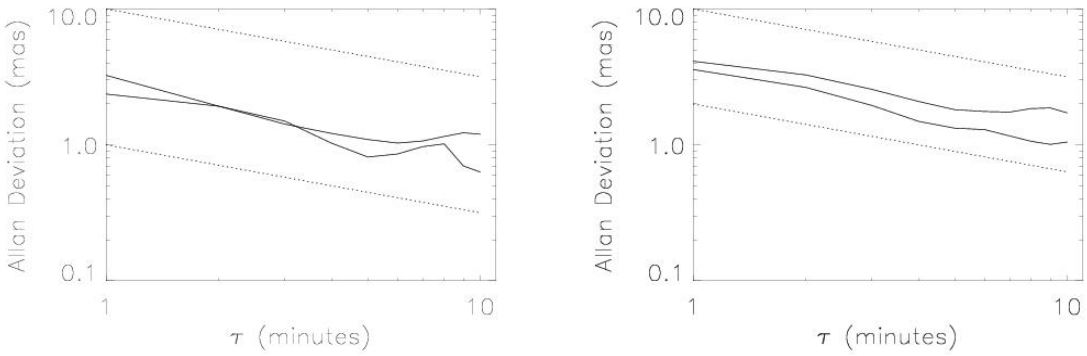

Figure 12: Allan deviation versus time for two representative stars in the narrow camera (*Top*) and the wide camera (*Bottom*).

of these objects.

The target fields are dense by conventional standards (5-100 stars per 10 arcsecond field), but have orders of magnitude less crowding than the Galactic center case (see above). Thus it represents a more 'typical' observing scenario that is encountered by astrometrists. Here we summarize the current astrometric precision and stability achieved by this program.

We can estimate our the precision of a single epoch of data by computing the distance from a target star to each of the reference stars (the 'grid') in our image. If our data are limited by random errors than the Allan deviation (the square root of the variance after averaging over various timescales) of each of these series of differences should decrease at $1/\sqrt{t}$. If the Allan deviation ceases to decrease in this fashion the data are limit by systematics.

Without the benefit of the new distortion solution (see above), the astrometric precision is limited to $\gtrsim 10 - 20$ mas, and there is no benefit of averaging. However, applying this new solution allows us to achieve ≈ 1 mas astrometry in both cameras (Figure 12), within a single epoch, and is stable at this level over the last 9 months. We are investigating the cause of this floor at ≈ 1 mas, but it is at the level where we expect residual uncorrected distortion, atmospheric refraction and tilt jitter to enter the data.

The systematic error in computing the geometric transformation from epoch-to-epoch is currently the largest factor limiting or astrometric accuracy. This is likely due to uncorrected differential chromatic refraction as seen in Figure 13. These effects are limiting our wide camera accuracy to ≈ 5 mas accuracy over year long timescales.

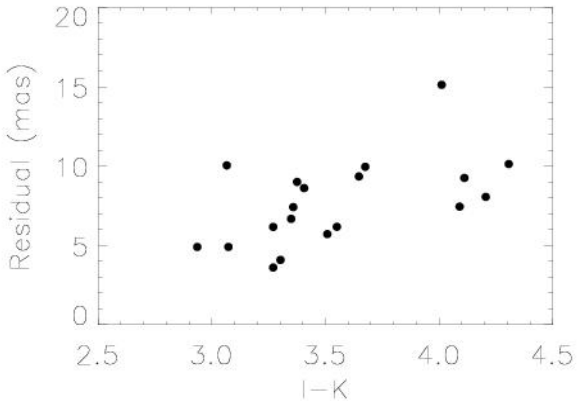

Figure 13: Differential chromatic refraction between to epochs in the field of magnetar 4U 0142+61.

4 Summary

Astrometry is one of the most powerful applications of adaptive optics, but it is still in its infancy. Astrometric studies will be concerned not only with the quality of the PSF delivered by the AO system, but also where it falls on the science instrument's detector. This is determined by uncorrected atmospheric turbulence, refraction and unavoidable optical distortions, each of which is in the process of being quantified, monitored and calibrated.

Relative astrometric precision at the level of ≈ 0.1 mas has already been achieved, and the photon noise limit has not yet been reached in many cases. Our current characterization of the geometric distortion in NIRC2 has yield the most substantial improvements in astrometric accuracy. To make the next leap in precision we will need to address issues of PSF variability, further characterization of the optical distortion and refraction effects.

5 Recommendations

Our current astrometric accuracy and precision is limited by our imperfect knowledge of the PSF, inability to characterize the optical distortion in the Keck telescope+AO optics and refraction effects. To this end, we suggest several tools that NGAO could provide for good astrometry, in addition to requirements for specific NGAO science cases.

- Require turbulence monitoring capabilities that deliver C_n^2 measurement on minute timescales. Measurements from a turbulence monitor will establish a baseline of C_n^2 profiles that may be used to understand both mean turbulence conditions and its degree of variability. This will help to establish expectations for astrometric stability. An understanding of the turbulence conditions under which NGAO is operating will significantly aid both operators and observers in making decisions on target selection and observing strategy. Use of turbulence profiles in post-processing algorithms also shows promise in improving astrometric precision.

- Consider providing an auxiliary camera for contemporaneous measurements of the PSF. The purpose of this camera would be to perform observations of a reference point source to provide the optical transfer function for use in post-processing algorithms which are currently under development. The exact requirements on this camera would depend upon the adaptive optics architecture selected for NGAO and the photometric requirements ultimately placed on the system. But to be useful this camera should be Nyquist sampled and should be deployable independently of the science detector. This camera should also be deployable over a field large enough to find a point source reference for PSF calibration.

- Require the ability to solve for and monitor optical distortion in the AO system and science instrument. Examples would be a well-machined pin hole slit mask placed as far upstream in the optical path as possible, or possibly a grid of fibers. It must be possible to rotate and translate either of these elements to solve simultaneously for their positions and the optical distortions. It is may also be possible to achieve this goal with on-sky tests, but work in this area is on-going.

- Consider providing an atmospheric dispersion corrector (ADC). This element must be driven as the telescope tracks (in contrast to the ADC at VLT which is preset at a given zenith distance). However, little work has been done to quantify the accuracy of the correction provided by these devices for astrometry, so we can not be certain as to whether such a device would make identifying and correcting residual atmospheric refraction more difficult.

- The current generation AO system provides a stable plate scale (changes by $\lesssim 1 \times 10^{-4}$ on timescales of a night). Some AO architectures (i.e. MCAO) could yield significantly worse plate scale stability due to unsensed modes between deformable mirrors, which lead to overall field (de)magnification. The timescales over which these modes operate are currently unknown, and will likely be a function of the system architecture and control loop design. Such field magnifications will be an

obstacle to high precision astrometry, particularly in spares fields where targets cannot be detected in a single image. Thus we require plate scale stability at the level of the current generation system.

- In order to achieve astrometric bias $\lesssim 0.1$ mas, our preliminary studies show that WFE ≈ 140 nm are required. Thus, NGAO should consider this level of WFE to achieve this particular science goal.

References

[1] L. Lindegren, "Photoelectric astrometry - A comparison of methods for precise image location," in *IAU Colloq. 48: Modern Astrometry*, F. V. Prochazka and R. H. Tucker, eds., pp. 197–217, 1978.

[2] D. G. Monet, C. C. Dahn, F. J. Vrba, H. C. Harris, J. R. Pier, C. B. Luginbuhl, and H. D. Ables, "U.S. Naval Observatory CCD parallaxes of faint stars. I - Program description and first results," *AJ* **103**, pp. 638–665, Feb. 1992.

[3] J. Gubler and D. Tytler, "Differential Atmospheric Refraction and Limitations on the Relative Astrometric Accuracy of Large Telescopes," *PASP* **110**, pp. 738–746, June 1998.

[4] K. C. Chambers, "Astrometry with Pan-STARRS and PS1: Pushing the limits of atmospheric refraction, dispersion, and extinction corrections for wide field imaging.," in *ASP Conf. Ser. 338: Astrometry in the Age of the Next Generation of Large Telescopes*, P. K. Seidelmann and A. K. B. Monet, eds., pp. 134–+, Sept. 2005.